

Helicon Oscillations in a Sphere

G. W. Ford

Physics Department, University of Michigan, Ann Arbor, Michigan 48104

S. A. Werner

Physics Department, Scientific Research Staff, Ford Motor Company, Dearborn, Michigan 48121

Department of Nuclear Engineering, University of Michigan, Ann Arbor, Michigan 48105

(Received 18 June 1973)

The helicon-wave problem is solved exactly for a sphere having an isotropic conductivity. The method involves the construction of a complete set of solutions of the helicon wave equation in spherical coordinates, a coordinate system in which the equation is not separable. Fitting the boundary condition at the surface of the sphere results in an expression for the induced ac magnetic multipole moments in the form of a ratio of two infinite determinants. Numerical results are presented for the induced dipole moment as a function of frequency and the strength of the applied dc magnetic field. A classification of the resonances in the dipole moment is proposed, and a table of resonant frequencies is given. Representative results for the induced octupole moment are displayed. The even- l 2^l -pole moments are zero. A preliminary comparison with the resonant frequencies observed by Rose with Na spheres in a field of 50 kG and with our own data on a small K sphere in a field of 2.5 kG shows an excellent agreement.

I. INTRODUCTION

Low-frequency electromagnetic oscillations of a plasma in the presence of a magnetic field have long been of interest.¹ When the plasma is the electron gas of a metal or semiconductor these oscillations are called helicons, and they have proved to be an important and useful probe for studying the electrical properties of solids at low temperatures. Maxfield gave in 1969 a review of the theory and some of the experimental techniques which is an excellent introduction to the helicon problem.² The experiments are always done by placing a sample in a dc magnetic field and exciting helicon current oscillations with a weak time-varying magnetic field. The difficulty has been that although such experiments are necessarily done on samples of finite size, no exact solution of the electromagnetic boundary value problem previously has been obtained for any finite geometry sample.

The purpose of this paper is to present an exact solution of the helicon problem for the sphere. This problem is not separable in spherical coordinates because of the presence of the Hall term in the conductivity, and this is the source of its difficulty. An obvious approach is to use the separability in Cartesian or cylindrical coordinates and fit the boundary conditions with a superposition of, say, plane waves. We have, however, chosen instead to attack the problem directly by constructing a complete set of solutions in spherical coordinates. The application of the boundary conditions then is straightforward.

In Sec. II we write the basic equations for the helicon waves and exhibit the known solutions for two cases: plane waves in an infinite medium and

the sphere with no dc magnetic field.³ In Sec. III we first construct the complete set of solutions in spherical coordinates. Writing the general solution as a superposition of these functions we determine the particular solution for the sphere by fitting the boundary conditions. The result is an expression for the induced magnetic multipole moments, in the form of a ratio of two infinite determinants. In Sec. IV we evaluate this expression in the limits of high and low frequencies and of zero dc magnetic field, recovering results obtained by other methods. Section V is devoted to the numerical evaluation of the expressions for the induced moments and a discussion of the results. Components of the induced ac magnetic dipole moment are plotted as functions of the dc magnetic field and the exciting frequency, tables of resonant frequencies are given, and selected results for the induced ac octupole moment are displayed. In Sec. VI we give a brief comparison of the theory with some preliminary experimental results, and finally, in Sec. VII make some concluding remarks on possible extensions of our work. In Appendices A, B, and C we collect a number of useful formulas on spherical Bessel functions, vector spherical harmonics, and the coupling of simple coil configurations to dipole and octupole fields.

II. BASIC EQUATIONS, ELEMENTARY SOLUTIONS

A. Helicon-Wave Equations

Helicons are low-frequency solutions of Maxwell's equations for the special case of a highly conducting medium in the presence of a strong applied dc magnetic field. For fields varying as $e^{-i\omega t}$ Maxwell's equations (in Gaussian units) reduce to

Faraday's law

$$\text{curl } \vec{E} = (i\omega/c) \vec{B} , \quad (1)$$

and Ampere's circuital law (for a medium of unit magnetic permeability)

$$\text{curl } \vec{B} = (4\pi/c) \vec{j} . \quad (2)$$

In Ampere's law we have neglected the displacement current, which is a very good approximation at the low frequencies of interest.²

The connection between the electric field and the current density is the Ohm-Hall law,

$$\sigma \vec{E} = \vec{j} + \omega_c \tau \hat{z} \times \vec{j} , \quad (3)$$

where σ is the conductivity, τ is the carrier relaxation time, and $\omega_c (= eB_0/mc)$ is the cyclotron frequency for the carriers of charge e and mass m in the dc magnetic field \vec{B}_0 , whose direction without loss of generality has been taken to be the positive z axis. (Note that ω_c is negative for electrons.) In the cyclotron frequency we neglect the small contribution of the ac magnetic field. The Hall coefficient $R_H = \omega_c \tau / \sigma B_0$ in this notation.

Eliminating the electric field \vec{E} between (1) and (3) we get

$$\vec{B} = (c/i\omega\sigma) \text{curl}(\vec{j} + \omega_c \tau \hat{z} \times \vec{j}) . \quad (4)$$

Inserting this expression in (2) we get

$$\text{curl} \text{curl}(\vec{j} + \omega_c \tau \hat{z} \times \vec{j}) - q_0^2 \vec{j} = 0 , \quad (5)$$

where the complex wave vector q_0 is given by

$$q_0^2 = i(4\pi\omega\sigma/c^2) . \quad (6)$$

Equation (4) together with (5), which we call the *helicon-wave equation*, constitute the basic equations describing the helicon.

For a finite sample, the field outside the sample is governed by the equations

$$\text{curl } \vec{B} = 0, \text{ div } \vec{B} = 0 . \quad (7)$$

The boundary condition is that the magnetic field \vec{B} is continuous at the surface of the sample.

B. Plane-Wave Solutions

If we seek plane-wave solutions of the form

$$\vec{j} = \vec{j}_{\vec{q}} e^{i\vec{q} \cdot \vec{r}} , \quad (8)$$

the helicon-wave equation becomes

$$(q^2 - q_0^2) \vec{j}_{\vec{q}} + q^2 \omega_c \tau (\hat{q} \cdot \hat{z}) \hat{q} \times \vec{j}_{\vec{q}} = 0 . \quad (9)$$

Thus, $\hat{q} \cdot \vec{j}_{\vec{q}} = 0$; the waves are transverse. Solutions of this homogeneous equation exist if and only if the wave vector \vec{q} satisfies the dispersion relation

$$q^2 = q_0^2 / (1 - i\lambda\omega_c\tau) , \quad (10)$$

where

$$\lambda = \pm \hat{q} \cdot \hat{z} . \quad (11)$$

The solutions are then (apart from a multiplicative amplitude factor)

$$\vec{j}_{\vec{q}} = \hat{z} - \hat{q} \cdot \hat{z} \hat{q} \pm i\hat{q} \times \hat{z} . \quad (12)$$

The simplest boundary value problem for which these plane-wave solutions are useful is that of an infinite slab with the dc field perpendicular to the slab and a uniform ac magnetic field lying in the plane of the slab. A superposition of four plane waves of the type given by (8) provides an exact solution. For details of this see Maxfield's paper.² To satisfy the boundary conditions for a sphere an infinite number of waves of the form (8) would be required.

C. Low Field Limit

In order to gain some additional insight we solve the helicon-wave equation for the sphere in the limit $\omega_c \tau = 0$, a problem whose solution is given in the book by Smythe.³ Consider a conducting sphere of radius a placed in a uniform ac magnetic field of amplitude \vec{B}_1 . Without loss of generality, we take \vec{B}_1 to be directed along the z axis. It is clear that the exciting ac magnetic field will induce eddy currents to circulate about the z axis. We therefore expect the current density \vec{j} to have only an azimuthal component.

A solution of (5) which has this symmetry is

$$\vec{j} = A j_1(q_0 r) \hat{z} \times \hat{r} . \quad (13)$$

Here j_1 is the spherical Bessel function (see Appendix A). The unknown coefficient A is to be determined from the boundary conditions. The simplest solution of Eqs. (7) for $\vec{B}(\vec{r})$ outside the sphere is the sum of the field of a dipole, of strength M , oriented in the z direction and the uniform applied ac magnetic field, that is,

$$\vec{B} = M[3(\hat{z} \cdot \hat{r})\hat{r} - \hat{z}]/r^3 + B_1 \hat{z} . \quad (14)$$

Using (13), the magnetic field inside the sphere is calculated from (4) and we find

$$\vec{B} = (c/3i\omega\sigma) A q_0 [j_2(q_0 r)(3\hat{z} \cdot \hat{r} \hat{r} - \hat{z}) + 2j_0(q_0 r) \hat{z}] , \quad (15)$$

where we have used the elementary properties of the spherical Bessel functions. Requiring that the magnetic field be continuous at the surface of the sphere, i. e., that the expressions (14) and (15) be equal at $r = a$, determines A and M :

$$A = \frac{3}{2} \frac{i\omega\sigma B_1}{c q_0 j_0(q_0 a)}, \quad M = \frac{1}{2} B_1 a^3 \frac{j_2(q_0 a)}{j_0(q_0 a)} . \quad (16)$$

Figure 1 shows the frequency dependence of the real and imaginary parts of this induced ac magnetic dipole moment. A detecting coil (or solenoid)

whose axis is along \hat{z} can be used to directly measure M . At low frequency $\text{Im}M$ is linear in ω , and $\text{Re}M$ is quadratic in ω , in fact,

$$\text{Im}M \approx (B_1 a^3 / 30) (4\pi\omega\sigma a^2 / c^2) \quad (17)$$

and

$$\text{Re}M \approx - (B_1 a^3 / 315) (4\pi\omega\sigma a^2 / c^2)^2. \quad (18)$$

Thus, at low frequency the ratio

$$\frac{\text{Re}M}{\text{Im}M} = -\frac{2}{21} \left(\frac{4\pi\omega\sigma a^2}{c^2} \right). \quad (19)$$

This ratio is independent of detector geometry and serves as a direct measure of the conductivity σ . Even in cases where $|q_0 a|$ is large and it is difficult to get into the low-frequency regime, the curves shown in Fig. 1 can be used to calculate the conductivity from the measured ratio of the out-of-phase to the in-phase signals. The technique has been successfully used previously.⁴

III. FORMAL SOLUTION OF HELICON PROBLEM FOR THE SPHERE

In this section we construct a complete set of solutions, regular at the origin, of Eq. (5) in spherical coordinates. We then write a complete set of solutions, regular at infinity, for Eqs. (7). Finally, we expand \vec{j} inside the sphere and \vec{B} outside the sphere in terms of these complete sets and determine the unknown coefficients by requiring that $\vec{B}(\vec{r})$ be continuous at the surface of the sphere.

A. Solution Inside the Sphere

To construct the *general solution*, regular at $r=0$, of Eq. (5) we introduce the vector function⁵:

$$\vec{A}_l^m(\vec{r}) = \left(\frac{l}{2l+1} \right)^{1/2} j_{l+1}(qr) \vec{Y}_{l,l+1}^m - \left(\frac{l+1}{2l+1} \right)^{1/2} j_{l-1}(qr) \times \vec{Y}_{l,l-1}^m, \quad (20)$$

$$\vec{B}_l^m(\vec{r}) = \left(\frac{l+1}{2l+1} \right)^{1/2} j_{l+1}(qr) \vec{Y}_{l,l+1}^m + \left(\frac{l}{2l+1} \right)^{1/2} j_{l-1}(qr) \times \vec{Y}_{l,l-1}^m, \quad (21)$$

$$\vec{C}_l^m(\vec{r}) = j_l(qr) \vec{Y}_{l,l}^m. \quad (22)$$

Here the j_l are spherical Bessel functions, and the $\vec{Y}_{l,l}^m$ are vector spherical harmonics. These special functions are discussed in Appendices A and B. The set of the \vec{A}_l^m , \vec{B}_l^m , \vec{C}_l^m (with $l=0, 1, 2, \dots$; $m=0, \pm 1, \dots, \pm l$; and the continuous parameter q) form a complete basis for vector functions of spherical coordinates. The members of this set are linearly independent and have been constructed so as to have the following simple vector analytical properties:

$$\text{div} \vec{A}_l^m = 0, \quad \text{div} \vec{B}_l^m = -q j_l(qr) Y_l^m, \quad \text{div} \vec{C}_l^m = 0, \quad (23)$$

and

$$\text{curl} \vec{A}_l^m = i q \vec{C}_l^m, \quad \text{curl} \vec{B}_l^m = 0, \quad \text{curl} \vec{C}_l^m = -i q \vec{A}_l^m. \quad (24)$$

These expressions follow directly from the formulas given in Appendices A and B. We will also need the following expressions:

$$\begin{aligned} \hat{z} \times \vec{A}_l^m &= i \sum_{l'} \left(-\frac{m}{l(l+1)} \delta_{ll'} \vec{A}_{l'}^m + \frac{m}{[l(l+1)]^{1/2}} \delta_{ll'} \vec{B}_{l'}^m - M_{ll'}^m \vec{C}_{l'}^m \right), \quad \hat{z} \times \vec{B}_l^m = i \sum_{l'} \left(\frac{m}{[l(l+1)]^{1/2}} \delta_{ll'} \vec{A}_{l'}^m + N_{ll'}^m \vec{C}_{l'}^m \right), \\ \hat{z} \times \vec{C}_l^m &= i \sum_{l'} \left(-\frac{m}{l(l+1)} \delta_{ll'} \vec{C}_{l'}^m + M_{ll'}^m \vec{A}_{l'}^m + L_{ll'}^m \vec{B}_{l'}^m \right), \end{aligned} \quad (25)$$

which have been obtained using Eq. (B15) in Appendix B for $\hat{z} \times \vec{Y}_{l,l}^m$. Here $\delta_{ll'}$ is the Kronecker δ , and

$$M_{ll'}^m = -\left(\frac{l(l+2)(l-m+1)(l+m+1)}{(l+1)^2(2l+1)(2l+3)} \right)^{1/2} \delta_{l',l+1} + \left(\frac{(l+1)(l-1)(l-m)(l+m)}{l^2(2l-1)(2l+1)} \right)^{1/2} \delta_{l',l-1}, \quad (26)$$

$$N_{ll'}^m = -[l(l+1)/l]^{1/2} M_{l,l+1} \delta_{l',l+1} + [l/(l+1)]^{1/2} M_{l,l-1} \delta_{l',l-1}, \quad (27)$$

$$L_{ll'}^m = -[l(l+1)/(l+2)]^{1/2} M_{l,l+1}^m \delta_{l',l+1} + [l/(l-1)]^{1/2} M_{l,l-1}^m \delta_{l',l-1}. \quad (28)$$

Turning now to the construction of the general solution of the helicon-wave equation, we begin by expanding the current density in the form

$$\vec{J} = \sum_l (a_l^m \vec{A}_l^m + c_l^m \vec{C}_l^m). \quad (29)$$

Here \vec{B}_l^m does not appear, since $\text{div} \vec{J} = 0$. Then, using (25) we have

$$\vec{J} + \omega_c \tau \hat{z} \times \vec{J} = \sum_{l,l'} [(a_l^m \{1 - i\omega_c \tau [m/l(l+1)]\} \delta_{ll'} + i\omega_c \tau c_l^m M_{ll'}^m) \vec{A}_{l'}^m + i\omega_c \tau (a_l^m \{m/[l(l+1)]^{1/2}\} \delta_{ll'} + c_l^m L_{ll'}^m) \vec{B}_{l'}^m$$

$$+ (c_l^m \{1 - i\omega_c \tau [m/l(l+1)]\} \delta_{ll'} - i\omega_c \tau a_l^m M_{ll'}^m) \bar{C}_l^m, \quad (30)$$

and then, using (24) we have

$$\text{curl}(J + \omega_c \tau \hat{z} \times \vec{J}) = iq \sum_{l,l'} [(a_l^m \{1 - i\omega_c \tau [m/l(l+1)]\} \delta_{ll'} + i\omega_c \tau c_l^m M_{ll'}^m) \bar{C}_l^m - (c_l^m \{1 - i\omega_c \tau [m/l(l+1)]\} \delta_{ll'} - i\omega_c \tau a_l^m M_{ll'}^m) \bar{A}_l^m]. \quad (31)$$

Finally, using (24) once again the helicon-wave equation becomes

$$0 = \text{curl curl}(\vec{J} + \omega_c \tau \hat{z} \times \vec{J}) - q_0^2 \vec{J} = \sum_{l,l'} [(a_l^m \{q^2 - q_0^2 - i\omega_c \tau q^2 [m/l(l+1)]\} \delta_{ll'} + i\omega_c \tau q^2 c_l^m M_{ll'}^m) \bar{A}_l^m + (c_l^m \{q^2 - q_0^2 - i\omega_c \tau q^2 [m/l(l+1)]\} \delta_{ll'} - i\omega_c \tau q^2 a_l^m M_{ll'}^m) \bar{C}_l^m]. \quad (32)$$

Since \bar{A}_l^m and \bar{C}_l^m are linearly independent, their coefficients in this equation must separately vanish. If we put

$$q^2 = \frac{q_0^2}{1 - i\lambda \omega_c \tau}, \quad (33)$$

these conditions become

$$\left. \begin{aligned} \sum_{l'} (\{\lambda - [m/l(l+1)]\} \delta_{ll'} a_l^m - M_{ll'}^m c_l^m) &= 0, \\ \sum_{l'} (\{\lambda - [m/l(l+1)]\} \delta_{ll'} c_l^m + M_{ll'}^m a_l^m) &= 0, \end{aligned} \right\} (l = |m|, |m| + 1, \dots) \quad (34)$$

where we have used the antisymmetry of $M_{ll'}^m$. For each m this is an infinite set of coupled homogeneous linear equations for the coefficients a_l^m and c_l^m . For every value of λ for which these equations have a nontrivial solution there is a corresponding solution \vec{J}_λ^m of Eq. (5).

Note that $M_{ll'}^m$ connects only values of l with opposite parity. Hence, the solutions of (34) are of two kinds: Even, for which $c_l^m = 0$ for odd l and $a_l^m = 0$ for even l ; and odd, for which $a_l^m = 0$ for odd l and $c_l^m = 0$ for even l . We will only be interested in the odd solutions. (A uniform ac magnetic field does not couple to the even solutions.) We therefore put

$$d_l^m = \begin{cases} c_l^m, & l \text{ odd} \\ a_l^m, & l \text{ even} \end{cases}. \quad (35)$$

Equation (34) can then be written as an infinite matrix eigenvalue problem:

$$\sum_{l'} (K_{ll'}^m - \lambda \delta_{ll'}) d_{l'}^m = 0, \quad (36)$$

where

$$K_{ll'}^m = [m/l(l+1)] \delta_{ll'} + (-)^l M_{ll'}^m. \quad (37)$$

The matrix whose elements are $K_{ll'}^m$ is real and symmetric; the eigenvalues λ will therefore all be real, and corresponding to each λ and its corresponding eigenvector $d_l^m(\lambda)$ we have a solution of (5) given by

$$\vec{J}_\lambda^m = \sum_{l \text{ odd}} d_l^m(\lambda) \bar{C}_l^m + \sum_{l \text{ even}} d_l^m(\lambda) \bar{A}_l^m. \quad (38)$$

Note that the eigenvectors $d_l^m(\lambda)$ appearing in this equation are independent of the two parameters $\omega_c \tau$ and q_0^2 ; they are simply the solutions of the eigenvalue problem posed in (36).

Supposing for the moment we have solved this eigenvalue problem, then the general odd-parity solution of the helicon-wave equation may be written as the superposition

$$\vec{J}(r) = \frac{c}{4\pi} \sum_{\lambda, m} q G_\lambda^m \vec{J}_\lambda^m. \quad (39)$$

Inserting this result into Eq. (4), and using (31), (34), and (35) we obtain for the magnetic field inside the sphere

$$\vec{B}(\vec{r}) = i \sum_{\lambda, m} G_\lambda^m \left(- \sum_{l \text{ odd}} d_l^m(\lambda) \bar{A}_l^m + \sum_{l \text{ even}} d_l^m(\lambda) \bar{C}_l^m \right). \quad (40)$$

The coefficients G_λ^m are to be determined from the boundary condition that the magnetic field inside the sphere must equal the magnetic field outside the sphere at $r = a$. In Sec. III B we write the general solution for \vec{B} outside the sphere.

B. Solution Outside the Sphere

Using the formulas for div and curl given in Appendix B, it can be verified that the vector functions

$$r^{-l-2} \vec{Y}_{l, l+1}^m; \quad \begin{aligned} l &= 0, 1, \dots \\ m &= 0, \pm 1, \dots, \pm l \end{aligned} \quad (41)$$

are solutions, regular at infinity, of Eqs. (7). The magnetic field outside the sphere must be the sum of a uniform exciting ac magnetic field \vec{B}_1 and an induced magnetic field which is a superposition of the vector functions (41). That is,

$$\vec{B} = \sum_{l, m} F_l^m (a/r)^{l+2} \vec{Y}_{l, l+1}^m + \vec{B}_1. \quad (42)$$

The constant vector \vec{B}_1 may be expressed in terms of the vector spherical harmonics. From Eq. (B4) of Appendix B we see that

$$\vec{Y}_{1,0}^m = (4\pi)^{-1/2} \hat{e}_m, \tag{43}$$

where the unit vectors \hat{e}_m are

$$\hat{e}_1 = -(2)^{-1/2}(\hat{x} + i\hat{y}), \quad \hat{e}_0 = \hat{z}, \quad \hat{e}_{-1} = (2)^{-1/2}(\hat{x} - i\hat{y}). \tag{44}$$

Thus,

$$\vec{B}_1 = (4\pi)^{1/2} \sum_{m=-1}^{+1} \hat{e}_m^* \cdot \vec{B}_1 \vec{Y}_{1,0}^m. \tag{45}$$

C. Satisfying Boundary Conditions

The magnetic field must be continuous at the surface of the sphere. Therefore the expressions (40) and (42) must be equal at $r = a$, that is

$$\sum_{\lambda, m} G_\lambda^m \left(\sum_{l \text{ odd}} d_l^m(\lambda) \vec{A}_l^m - \sum_{l \text{ even}} d_l^m(\lambda) \vec{C}_l^m \right)_{r=a} = i \left(\sum_{l, m} F_l^m \vec{Y}_{l, l+1}^m + (4\pi)^{1/2} \sum_{m=-1}^1 \hat{e}_m^* \cdot \vec{B}_1 \vec{Y}_{1,0}^m \right). \tag{46}$$

This relation determines the coefficients G_λ^m and F_l^m . Using the expressions (20) and (22) for \vec{A}_l^m and \vec{C}_l^m and the orthogonality of the $\vec{Y}_{L,l}^m$, we obtain

$$F_l^m = \begin{cases} -i \left(\frac{l}{2l+1} \right)^{1/2} \sum_\lambda G_\lambda^m d_\lambda^m(\lambda) j_{l+1}(qa), & l \text{ odd} \\ 0, & l \text{ even} \end{cases} \tag{47}$$

which follows from the equality of the coefficients of $\vec{Y}_{l, l+1}^m$, and

$$\sum_\lambda G_\lambda^m d_l^m(\lambda) \times \begin{cases} j_{l-1}(qa), & l \text{ odd} \\ j_l(qa), & l \text{ even} \end{cases} = -i(6\pi)^{1/2} \hat{e}_m^* \cdot \vec{B}_1 \delta_{l1}, \tag{48}$$

which follows from the equality of the coefficients of $\vec{Y}_{l, l-1}^m$ and $\vec{Y}_{l, l}^m$. We should emphasize that q depends upon λ through (33), that is,

$$qa = \left(\frac{i 4\pi\omega\sigma a^2/c^2}{1 - i\lambda\omega_c\tau} \right)^{1/2}. \tag{49}$$

Here the choice of the sign of the square root does not matter since only spherical Bessel functions of even order occur in (47) and (48).

Equation (48) is an infinite set of inhomogeneous linear equations for the determination of G_λ^m . Note that the coefficients G_λ^m for different m are not coupled together, and also that G_λ^m is zero for $|m| > 1$. The matrix of coefficients in these equations is

$$X_{lk}^m = d_l^m(\lambda_k) \times \begin{cases} j_{l-1}(q_k a), & l \text{ odd} \\ j_l(q_k a), & l \text{ even} \end{cases}, \tag{50}$$

in which the rows are labeled by l and the columns by the eigenvalues $\lambda_k (k=1, 2, \dots)$ determined from (36). By Cramer's rule⁶ the solution of (48) is

$$G_{\lambda_k}^m = -i(6\pi)^{1/2} \hat{e}_m^* \cdot \vec{B}_1 \frac{\text{cofactor}(X_{lk}^m)}{\det(X_{lk}^m)}. \tag{51}$$

Inserting this result in (47) we have

$$F_l^m = - \left(\frac{6\pi l}{2l+1} \right)^{1/2} \hat{e}_m^* \cdot \vec{B}_1 \times \frac{\begin{vmatrix} d_1^m(\lambda_1)j_{l+1}(q_1a) & d_1^m(\lambda_2)j_{l+1}(q_2a) & d_1^m(\lambda_3)j_{l+1}(q_3a) & d_1^m(\lambda_4)j_{l+1}(q_4a) & \dots \\ d_2^m(\lambda_1)j_2(q_1a) & d_2^m(\lambda_2)j_2(q_2a) & d_2^m(\lambda_3)j_2(q_3a) & d_2^m(\lambda_4)j_2(q_4a) & \dots \\ d_3^m(\lambda_1)j_2(q_1a) & d_3^m(\lambda_2)j_2(q_2a) & d_3^m(\lambda_3)j_2(q_3a) & d_3^m(\lambda_4)j_2(q_4a) & \dots \\ d_4^m(\lambda_1)j_4(q_1a) & d_4^m(\lambda_2)j_4(q_2a) & d_4^m(\lambda_3)j_4(q_3a) & d_4^m(\lambda_4)j_4(q_4a) & \dots \\ \vdots & \vdots & \vdots & \vdots & \dots \\ \vdots & \vdots & \vdots & \vdots & \dots \\ \vdots & \vdots & \vdots & \vdots & \dots \end{vmatrix}}{\begin{vmatrix} d_1^m(\lambda_1)j_0(q_1a) & d_1^m(\lambda_2)j_0(q_2a) & d_1^m(\lambda_3)j_0(q_3a) & d_1^m(\lambda_4)j_0(q_4a) & \dots \\ d_2^m(\lambda_1)j_2(q_1a) & d_2^m(\lambda_2)j_2(q_2a) & d_2^m(\lambda_3)j_2(q_3a) & d_2^m(\lambda_4)j_2(q_4a) & \dots \\ d_3^m(\lambda_1)j_2(q_1a) & d_3^m(\lambda_2)j_2(q_2a) & d_3^m(\lambda_3)j_2(q_3a) & d_3^m(\lambda_4)j_2(q_4a) & \dots \\ d_4^m(\lambda_1)j_4(q_1a) & d_4^m(\lambda_2)j_4(q_2a) & d_4^m(\lambda_3)j_4(q_3a) & d_4^m(\lambda_4)j_4(q_4a) & \dots \\ \vdots & \vdots & \vdots & \vdots & \dots \\ \vdots & \vdots & \vdots & \vdots & \dots \\ \vdots & \vdots & \vdots & \vdots & \dots \end{vmatrix}}. \tag{52}$$

Here the denominator is the determinant of the matrix X_{lk}^m given in (50) while the numerator is the determinant of the same matrix but with the first row replaced by $d_l^m(\lambda_k)j_{l+1}(q_k a)$; $k=1, 2, \dots$. This completes the formal solution of the problem.

D. Auxiliary Eigenvalue Problem

In order to evaluate the ratio of the determinants given in Eq. (52) we must first solve the auxiliary eigenvalue problem (36). The exact solution to this problem is that the eigenvalues λ are continu-

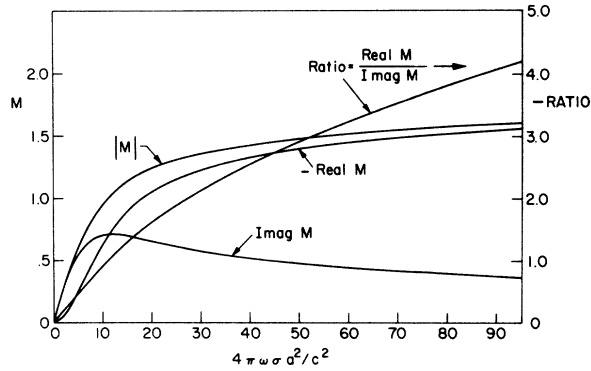


FIG. 1. Induced ac magnetic dipole moment M as given by Eq. (16) as a function of $|q_0 a|^2 = 4\pi\omega\sigma a^2/c^2$. The applied dc field is zero. (In mks units $|q_0 a|^2 = \mu_0\omega\sigma a^2$.)

ously distributed in the interval

$$-1 \leq \lambda \leq 1, \quad (53)$$

and the eigenvectors are

$$d_l^m(\lambda) = \begin{cases} (-)^{(l-1)/2}, & l \text{ odd} \\ (-)^{(l-2)/2}, & l \text{ even} \end{cases} \\ \times \left(\frac{(2l+1)(l-1)!(l+1)!}{8(l+m)!(l-m)!} \right)^{1/2} (1+\lambda)^{(3+2m)/4} \\ \times (1-\lambda)^{(3-2m)/4} P_{l-1}^{(1-m, 1+m)}(\lambda), \quad (54)$$

where $P_n^{(\alpha, \beta)}(\lambda)$ is the Jacobi polynomial.⁷ These eigenvectors are closely related to the functions $d_m^{(j), m}$ occurring in the irreducible representation of finite rotations.⁸ The fact that (54) solves the eigenvalue problem (36) can be directly verified using the recurrence relation for the Jacobi polynomials given in Ref. 7 (p. 169). The eigenvalues λ can be interpreted as the cosine of an angle, namely,

$$\lambda = \cos \theta, \quad (55)$$

which shows the connection between the definition (33) and the dispersion relation (10) for plane waves of wave vector \vec{q} . The eigenvectors given in (54) form a complete orthonormal set of functions in the interval $[0, \pi]$, thus

$$\sum_l d_l^m(\lambda) d_l^m(\lambda') = \delta(\theta - \theta'), \quad (56)$$

$$\int_0^\pi d\theta d_l^m(\lambda) d_l^m(\lambda) = \delta_{ll'},$$

where $\delta(\theta - \theta')$ is the Dirac δ .

Clearly there is a problem in the evaluation of the infinite determinants in (52), in which the columns are labeled by the continuous index λ . There

are a number of approaches to this problem. One is to multiply on the right-hand side both numerator and denominator matrices in (52) by, say, the transpose of the denominator matrix. (This does not change the ratio of the determinants.) Both rows and columns in the resulting matrix are labeled by l ; the matrix elements are integrals over λ . This is in fact equivalent to transforming Eq. (48) into an integral equation and solving by the Fredholm method.⁹

The method we have used is somewhat different, and seems to be computationally simpler. We truncate the eigenvalue problem (36) by replacing the infinite matrix $K_{ll'}$ by its $N \times N$ upper-left-hand corner. The eigenvalues of the truncated problem are then discrete: $\lambda_k (k = 1, 2, \dots, N)$. They all lie in the interval $-1 \leq \lambda_k \leq 1$. The eigenvectors satisfy the orthogonality and completeness relations:

$$\sum_{l=1}^N d_l^m(\lambda_k) d_l^m(\lambda_{k'}) = \delta_{kk'}, \quad (57)$$

$$\sum_{k=1}^N d_l^m(\lambda_k) d_{l'}^m(\lambda_k) = \delta_{ll'}.$$

As N becomes large the eigenvalues fill the interval $-1 \leq \lambda_k \leq 1$ densely, and the corresponding eigenvectors become asymptotically equivalent to (54), aside from a normalization factor.

For this truncated problem the determinants in Eq. (52) are of size $N \times N$, their ratio approaching the ratio of the infinite determinants as N approaches infinity. In practice we find reasonable numerical convergence for N as small as 1; however, to obtain accurate results we have used N as large as 15.

E. Induced ac Magnetic Moments

The induced magnetic dipole moment is given by

$$\vec{M}(\omega) = -a^3 (8\pi)^{-1/2} \sum_{m=-1}^1 F_1^m \hat{e}_m, \quad (58)$$

which can be obtained by comparing the $l=1$ terms in (42) with the usual expression for the magnetic field of a dipole. The argument ω is explicitly shown to emphasize that these functions are defined in the frequency domain. The time dependence of the magnetic dipole moment, i. e., $\vec{M}(t)$, is found by multiplying by $e^{-i\omega t}$ and forming the real part.

Two cases are of special interest: (i) the transverse geometry where the applied ac and dc magnetic fields are mutually perpendicular, and (ii) the longitudinal geometry where these applied fields are collinear. We take the dc magnetic field along the z axis and for the transverse geometry the ac field along the x axis.

For the transverse geometry $F_1^0 = 0$, and the components of the magnetic dipole moment are

$$\begin{aligned} M_x(\omega) &= (a^3/4\pi^{1/2})(F_1^1 - F_1^{-1}) , \\ M_y(\omega) &= (ia^3/4\pi^{1/2})(F_1^1 + F_1^{-1}) , \\ M_z(\omega) &= 0 . \end{aligned} \quad (59)$$

Thus the induced dipole moment is always in the x - y plane, i. e., normal to the dc field \vec{B}_0 .

The vector $\vec{M}(t)$ will move on an ellipse in this plane. The eccentricity ϵ and the angle β between the major axis of this ellipse and the x axis are given by

$$\begin{aligned} \tan 2\beta &= -\frac{\text{Im}(F_1^1 F_1^{-1*})}{\text{Re}(F_1^1 F_1^{-1*})} , \\ \epsilon &= 2 \frac{(|F_1^1| |F_1^{-1}|)^{1/2}}{|F_1^1| + |F_1^{-1}|} . \end{aligned} \quad (60)$$

Here the asterisk(*) means complex conjugation.

For the longitudinal geometry the induced dipole moment is along \hat{z} and is given by

$$M_z(\omega) = -a^3(8\pi)^{-1/2} F_1^0 . \quad (61)$$

The behavior of the higher moments is similar to that of the dipole moment. The quadrupole moment ($l=2$), the hexadecapole moment ($l=4$), and all higher even- l 2^l -pole moments are zero. A vector moment in analogy with (58) can be defined for the higher odd- l 2^l -pole moments:

$$\vec{M}^{(l)} = -a^{l+2}(8\pi)^{-1/2} \sum_{m=-l}^l F_1^m \hat{e}_m . \quad (62)$$

The configuration of the induced current loops which give rise to the calculated octupole field are

shown in Fig. 2; the arrows indicate the direction perpendicular to the current loops, i. e., the equivalent magnetic dipole of each loop of circulating current. For the transverse case [Fig. 2(a)] the axis of the arrows rotates about \vec{B}_0 with frequency $\omega/2\pi$ in a manner completely analogous to the time dependence of the dipole moment. Thus, the octupole moment can also be viewed as describing an ellipse in the x - y plane as a function of time. The axis of the octupole moment in the longitudinal geometry is fixed (independent of time) and is always the z axis.

IV. RESULTS IN VARIOUS LIMITS

There are two parameters in our problem: The first is

$$V \equiv |q_0 a|^2 = 4\pi\omega\sigma a^2/c^2 (= \mu_0\omega\sigma a^2 \text{ in mks units}) , \quad (63)$$

which is a dimensionless measure of the frequency of the applied ac magnetic field. Note that V is (aside from a factor of 2) the square of the ratio of the radius of the sphere to the classical skin depth. The second parameter is

$$W \equiv \omega_c \tau = eB_0 \tau / mc , \quad (64)$$

which is a dimensionless measure of the dc magnetic field. In this section we obtain expressions for F_l^m in terms of these parameters in three limits: low frequency, high frequency, and zero dc magnetic field. The object here is to compare these expressions with known results in these limits.

A. Low Frequency

Consider first the case $l=1$ (dipole moment). In the first two rows of the numerator and denominator determinants of (52) we use the power series expansion of $j_n(qa)$ [Eq. (A4)], keeping only the first two terms. We then have

$$F_1^m \approx -\frac{(2\pi)^{1/2}}{15} \hat{e}_m^* \cdot \vec{B}_1 V \frac{\begin{vmatrix} \dots & x_j(1 - \frac{1}{14} Vx_j) d_1^m(\lambda_j) \dots \\ \dots & x_j(1 - \frac{1}{14} Vx_j) d_2^m(\lambda_j) \dots \\ & \vdots \end{vmatrix}}{\begin{vmatrix} \dots & (1 - \frac{1}{6} Vx_j) d_1^m(\lambda_j) \dots \\ \dots & x_j(1 - \frac{1}{14} Vx_j) d_2^m(\lambda_j) \dots \\ & \vdots \end{vmatrix}} , \quad (65)$$

where in the determinants we have indicated the typical elements in the first two rows, and

$$x_j = i/(1 - i\lambda_j W) . \quad (66)$$

We now rearrange the denominator determinant by

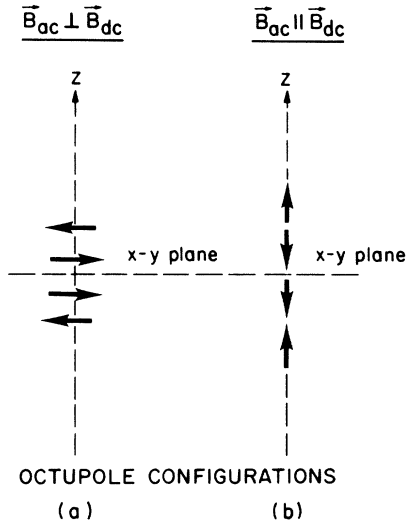


FIG. 2. Array of magnetic dipoles equivalent to the octupole moments. They are completely described by the vector moment given in Eq. (62).

multiplying each element of the second row by $W[20(4-m^2)]^{1/2}$, adding the result to the first row, and then using the first of the infinite set of equations (36):

$$d_2^m(\lambda_j) = -[20/(4-m^2)]^{1/2}(\frac{1}{2}m + i/W + 1/Wx_j)d_1^m(\lambda_j). \quad (67)$$

The typical element of the first row can then be written in the form

$$-\left(\frac{1}{2}mW + i + \frac{2}{21} \frac{V}{1 - \frac{1}{14}Vx_j}\right)x_j(1 - \frac{1}{14}Vx_j)d_1^m(\lambda_j). \quad (68)$$

But, neglecting terms of the order V^2 , this is just the factor

$$-(\frac{1}{2}mW + i + \frac{2}{21}V) \quad (69)$$

times the typical element of the first row of the numerator. Therefore,

$$F_1^m \approx \frac{(2\pi)^{1/2}}{15} \hat{e}_m^* \cdot \vec{B}_1 \frac{2V}{mW + 2i} \left(1 - \frac{4}{21} \frac{V}{mW + 2i}\right), \quad (70)$$

where again we have neglected terms of relative order V^2 .

Using (59), the components of the induced ac magnetic dipole moment for the transverse geometry are¹⁰

$$M_x = i \frac{2}{15} B_1 a^3 \frac{V}{4 + W^2} - \frac{4}{315} B_1 a^3 \frac{(4 - W^2)V^2}{(4 + W^2)^2} + \dots$$

$$M_y = -i \frac{1}{15} B_1 a^3 \frac{WV}{4 + W^2} + \frac{16}{315} B_1 a^3 \frac{WV^2}{(4 + W^2)^2} + \dots \quad (71)$$

$$M_z = 0.$$

Note that the imaginary and real parts of \vec{M} are, respectively, linear and quadratic in frequency.

Thus, if the frequency is sufficiently low, the induced ac magnetic dipole moment is 90° out of phase with the driving field.

When $W=0$, $M_y=0$, and the expression for M_x becomes the same as Eqs. (17) and (18). With increasing dc magnetic field $\text{Im}\vec{M}$ tips out of the x - z plane, with tipping angle

$$\tan^{-1}\left(\frac{\text{Im}M_y}{\text{Im}M_x}\right) = -\tan^{-1}\left(\frac{1}{2}W\right), \quad (72)$$

and at the same time this moment decreases monotonically. Note that $\text{Re}M_x$ changes sign at $W=2$, and $\text{Re}M_y$ has a maximum at $W=2/3^{1/2}$, effects which give a convenient measure of $W=\omega_c\tau$. We have experimentally observed these low-frequency effects in potassium at 4.2 K.

These results can also be applied to induced torque experiments in which the $\partial\vec{B}/\partial t$ is created by rotating field \vec{B}_0 at angular frequency ω about a fixed sample. If the axis of rotation is \hat{y} and the instantaneous direction of \vec{B}_0 is \hat{z} , then $\partial\vec{B}/\partial t = \omega B_0 \hat{x}$, and the y component of the torque is (in lowest order in V)

$$N_y = (\vec{M} \times \vec{B}_0)_y = \frac{8\pi\omega a^5 \sigma}{15 c^2} \frac{B_0^2}{4 + W^2}. \quad (73)$$

The frequencies involved in these experiments are always low enough so that the higher-order terms in V are negligible.¹¹

For the longitudinal geometry ($\vec{B}_1 \parallel \vec{B}_0$) the low-frequency expression for M_z obtained from (61) and (70) is¹⁰

$$M_z = i \frac{1}{30} B_1 a^3 V - \frac{1}{315} B_1 a^3 V^2 + \dots \quad (74)$$

Note that this result is independent of $\omega_c\tau$; and is therefore identical to the zero applied field results (17) and (18). Hence by measuring the ratio of the out-of-phase to the in-phase signals at low frequencies one can directly measure the magnetic field dependence of the conductivity, i. e., the magneto-resistance.

The leading term in the higher- l 2^l -pole moments depends on frequency as $\omega^{(l+1)/2}$, as is easily established directly from (52). Thus, as soon as the term quadratic in frequency becomes significant in the dipole moment, the octupole field begins to develop.

B. High Frequency

At very high frequency, the arguments of the spherical Bessel functions are large, so we can use the asymptotic form

$$j_n(q_1 a) \sim (-)^{n/2} \sin(q_1 a)/q_1 a, \quad n \text{ even}. \quad (75)$$

Thus, we can factor out $\sin(q_1 a)/q_1 a$ from each column in the numerator and denominator determinants of Eq. (52). In the remaining determinants we can factor -1 from those rows where the index of the

Bessel functions is twice an odd integer. For F_1^m this leaves the determinant of the matrix $d_i(\lambda_i)$ in both the numerator and denominator. Therefore

$$F_1^m \approx (2\pi)^{1/2} \hat{e}_m^* \cdot \vec{B}_1, \quad (76)$$

and the induced dipole moment is identical with the high-frequency limit of (16):

$$\vec{M} = -\frac{1}{2} a^3 \vec{B}_1. \quad (77)$$

The higher moments are zero in this limit, since for F_1^m , the first row of the numerator matrix is the same (up to a sign) as the l th row. We see then that at both low and high frequencies, the magnetic field due to the higher moments approaches zero asymptotically.

C. Zero dc Field

When $\omega_c \tau = 0$, the spherical Bessel functions can be factored from the rows of the determinants in Eq. (52) since their arguments $q_i a = q_0 a$, independent of the index i . For F_1^m this again leaves the determinant of the matrix $d_i(\lambda_i)$ in both numerator and denominator so

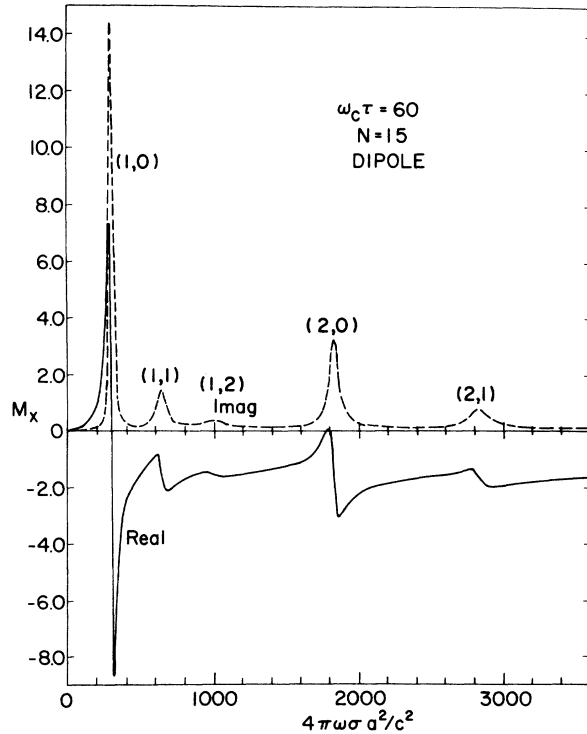


FIG. 3. Real and imaginary parts of M_x (in units of $\frac{1}{2} B_1 a^3$) as a function of $V = 4\pi\omega\sigma a^2/c^2$ for $W = \omega_c \tau = 60$ in the transverse geometry. The resonance indexing scheme is given by Eq. (80). Note that the calculation is done for positive $\omega_c \tau$, i. e., positive carriers. Changing the sign of W has the effect of changing the sign of M_x .

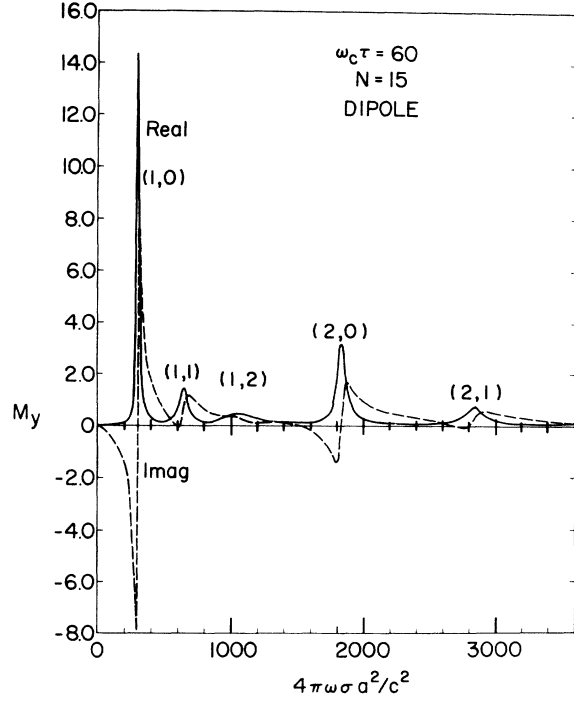


FIG. 4. Real and imaginary parts of M_y as a function of $V = 4\pi\omega\sigma a^2/c^2$ for $W = \omega_c \tau = 60$.

$$F_1^m = -(2\pi)^{1/2} \hat{e}_m^* \cdot \vec{B}_1 \frac{j_2(q_0 a)}{j_0(q_0 a)}. \quad (78)$$

The induced dipole moment is

$$\vec{M} = \frac{1}{2} a^3 \frac{j_2(q_0 a)}{j_0(q_0 a)} \vec{B}_1, \quad (79)$$

which agrees with (16). The higher moments vanish.

V. NUMERICAL RESULTS

Experimentally, one is interested in the magnetic induction field $\vec{B}(\vec{r})$ outside the sphere or, equivalently, the induced magnetic multipole moments. These are completely specified by the coefficients F_1^m which depend on the two parameters $V = 4\pi\omega\sigma a^2/c^2$ and $W = \omega_c \tau$. In this section we discuss the results of numerical calculations for these coefficients.

A. Transverse Geometry

In this geometry we take the strong dc magnetic field in the z direction and the applied ac magnetic field perpendicular to it in the x direction. The results of a representative calculation are shown in Figs. 3 and 4. There the real and imaginary parts of the x and y components of the induced dipole moment are plotted as a function of V for $\omega_c \tau = 60$. The series of peaks shown in these figures have an obvious structure: a large "fundamental" resonance at $V = 295$ followed by a number of smaller

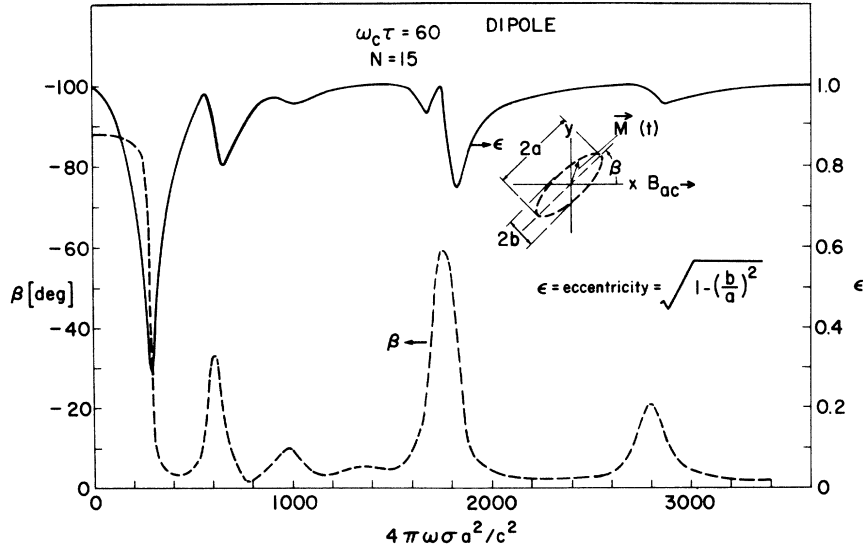


FIG. 5. Eccentricity ϵ and the angle β as given by Eqs. (60) as a function of V for $\omega_c\tau = 60$.

“satellites,” then another fundamental resonance at $V = 1820$, again followed by a number of satellites. This same structure persists and can be followed out to very large values of W . There the resonances can be neatly classified according to the structure of the magnetic field inside the sphere: We simply count the number of nodes in $\text{Im}(B_x + iB_y)$ along the z direction and then the x direction. The resulting pair of indices

$$(\text{number of nodes along } \hat{z}, \text{ number of nodes along } \hat{x}) \quad (80)$$

serve to label the resonances.¹² The peaks in Figs. 3 and 4 are labeled according to this scheme. Note that the fundamentals have second index zero and the satellites of each fundamental have the same value of the first index and second index = 1, 2, . . .

In Sec. III E we saw that the locus of the induced dipole moment $\vec{M}(t)$ is an ellipse in the xy plane, characterized by its eccentricity ϵ and the angle β between its major axis and the x axis. The dependence of ϵ and β on V is shown in Fig. 5, again for $\omega_c\tau = 60$. At very low frequencies $\epsilon \approx 1$ and the angle $\beta \approx -88^\circ$ ($= -\tan^{-1} \frac{1}{2} \omega_c\tau$), in agreement with the low-frequency results of Sec. IV A. At higher frequencies the resonant structure shown in Figs. 3 and 4 is reflected in the behavior of ϵ and β . The essential feature seems to be that the motion of $\vec{M}(t)$ becomes less eccentric at the resonances, and that between the resonances the moment is almost linearly polarized in the x direction. Of course, $\epsilon \rightarrow 1$, $\beta \rightarrow 0$ at high frequency in agreement with the results of Sec. IV B.

The development of resonant structure with increasing magnetic field is shown in Figs. 6 and 7, where $\text{Im}M_x$ and $\text{Re}M_y$ are plotted as functions of

V for various values of $\omega_c\tau$. For $\omega_c\tau = 0$, $M_y = 0$ and M_x is given by the low-frequency result (16). As $\omega_c\tau$ increases the low-frequency peak in $\text{Im}M_x$ sharpens and develops into the first fundamental helicon resonance peak. The frequency ω_r at which this peak occurs varies with $\omega_c\tau$ as shown in Fig. 8. At large values of $\omega_c\tau$ this peak frequency is asymptotically linear in $\omega_c\tau$; we find numerically

$$4\pi\omega_r\sigma a^2/c^2 = 4.9020\omega_c\tau (1 + 2.90/\omega_c^2\tau^2) . \quad (81)$$

The satellites and the higher fundamental peaks appear to grow out of the same zero field peak. The peak frequencies and the corresponding peak heights of all of the resonances become asymptotically linear in $\omega_c\tau$. It is interesting to note that the satellite structure continues to develop with increasing $\omega_c\tau$; even at $\omega_c\tau = 60$ the satellite peak (1, 3) is just visible. It appears that the complete resonant structure at very high $\omega_c\tau$ consists of three satellites between the first and second fundamentals, two satellites between the second and third, and one between the third and fourth. Table I contains a list of the high field limit of $4\pi\omega_r\sigma a^2/c^2\omega_c\tau$ for these resonances.

As indicated in Sec. III E we can characterize the induced magnetic octupole moment by a vector $\vec{M}^{(3)}$ whose components are

$$\begin{aligned} M_x^{(3)} &= (a^5/4\pi^{1/2})(F_3^1 - F_3^{-1}) , \\ M_y^{(3)} &= (ia^5/4\pi^{1/2})(F_3^1 + F_3^{-1}) . \end{aligned} \quad (82)$$

These moments are shown in Figs. 9 and 10 for $\omega_c\tau = 60$. There is clearly a connection between the resonant structures of the octupole and dipole moments, but it does not appear to be simple. Note that in the region between the first and second fundamental dipole resonances, the octupole field

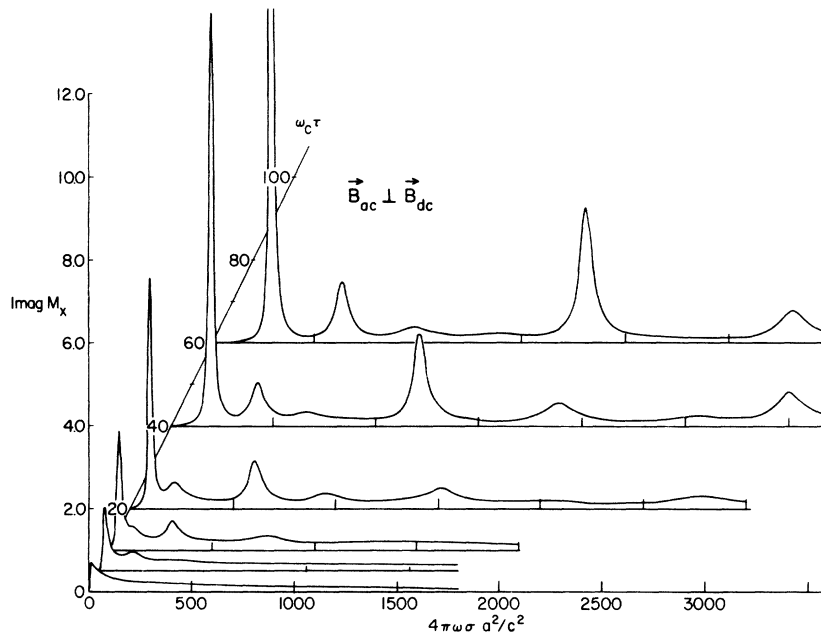


FIG. 6. Development of the helicon resonant structure with increasing dc field ($\omega_c \tau$) for the transverse geometry. $\text{Im}M_x$ is in units of $\frac{1}{4}B_1 a^3$. The lowest frequency peak is the first fundamental resonance, i. e., (1,0). It occurs at progressively higher frequencies as $\omega_c \tau$ is increased; its location in frequency is given by Eq. (81) at high $\omega_c \tau$, and by Fig. 8 for low $\omega_c \tau$. The calculations were done with $N=11$ for $\omega_c \tau \leq 20$ and with $N=15$ for $\omega_c \tau = 40$ and 60.

is comparable to or even larger than the dipole field.

B. Longitudinal Geometry

In the longitudinal geometry¹³ both the ac and dc applied fields are in the z direction. In Fig. 11 the imaginary part of M_z is plotted as a function of V for various values of $\omega_c \tau$. As in the transverse case there is again an obvious resonant structure.

The most striking differences are the absence of the large fundamental resonances and the fact that the low-frequency peak is essentially independent of $\omega_c \tau$. We already remarked in Sec. IV A that this latter feature permits a direct measure of the magneto-resistance; a change in signal level can occur only if σ is magnetic field dependent. In this geometry we classify the resonances in terms of the number of nodes in $\text{Im}B_z$ along the z direction and

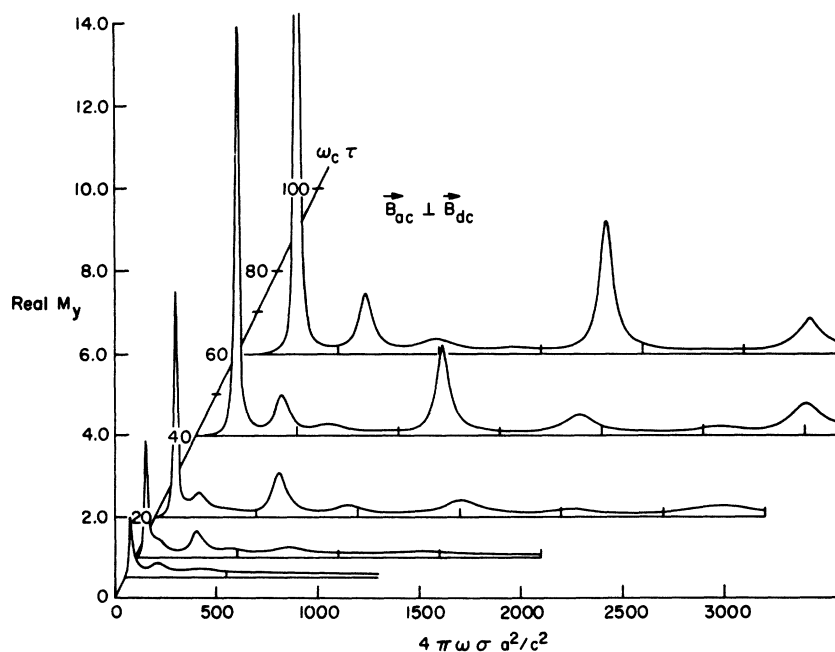


FIG. 7. Development of the helicon resonant structure with increasing $\omega_c \tau$ as observed in $\text{Re}M_y$. Note the similarity to Fig. 6.

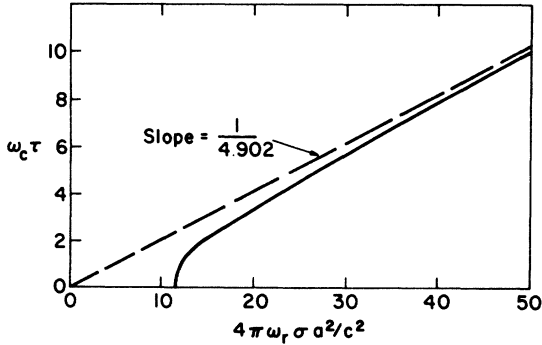


FIG. 8. $\omega_c \tau$ dependence of the position of the first helicon peak in the region of low $\omega_c \tau$.

then the x direction. That is to say the indexing rule (80) applies here as well. These indices are shown in Fig. 11. (We do not apply this indexing scheme to the low-frequency peak which is clearly of a different character.) These resonances are comparable in amplitude to their counterparts in the transverse case. The peak frequencies and amplitudes again are asymptotically linear in $\omega_c \tau$. For the (1, 1) resonance we find numerically

$$4\pi\omega_r\sigma a^2/c^2 = 21.781\omega_c\tau(1 + 3.83/\omega_c^2\tau^2) . \quad (83)$$

Table I contains a list of the high field limit of $4\pi\omega_r\sigma a^2/c^2\omega_c\tau$ for these longitudinal resonances.

C. Numerical Convergence

It is difficult to give a general rule for the speed of convergence in this problem. However, a number of reasonably general statements can be made.

The low-frequency results of Sec. IV A are independent of matrix size N . Thus, as long as one can neglect terms cubic in frequency, a calculation with $N=1$ yields very accurate results.

As the parameter V (frequency) increases, progressively larger matrix sizes must be used.

As the parameter W (dc magnetic field) increases progressively larger matrix sizes must be used.

Convergence occurs more rapidly for the fundamental resonances than for the satellite resonances for the transverse geometry. For the longitudinal geometry convergence occurs most rapidly for the (l, l) resonances. For example, the peak height of the (1, 0) transverse resonance is calculated to an accuracy of 1 part in 3000 for $N=5$ for values of $W \leq 1000$.

Higher multipoles require a somewhat larger matrix size. However, the octupole results shown in Figs. 9 and 10 calculated with $N=15$ are indistinguishable on the scale of the drawing from those calculated with $N=13$.

A more precise indication of the accuracy of our calculations can be obtained from Table II. This table contains values of V/W at resonance; for the transverse geometry the peak heights of $\text{Im}M_x$ are

in units of $\frac{1}{4}B_1a^3$, for the longitudinal geometry the peak heights of $\text{Im}M_z$ are in units of $\frac{1}{2}B_1a^3$.

It is clear that at some large matrix size, numerical divergence must occur since rounding errors become important. We have found that this divergence occurs in a rapid and obvious manner in the region $19 \leq N \leq 25$ depending on the choice of parameters V and W . All computations were done on a PDP-10 computer in single precision (eight significant figures) and require about 7 sec of CPU time for a given V and W for $N=15$.

VI. PRELIMINARY COMPARISON WITH EXPERIMENT

We show in Table III a comparison of the resonant frequencies observed by Rose¹⁴ in transverse-geometry helicon measurements on two spheres of sodium metal at 4.2 K in a field of 50 kG with the calculations presented in this paper. The frequencies are normalized to the (1, 0) resonance. The rms difference between theory and experiment is 3.9% for the 9.63-mm diameter sphere and 2.8% for the 6.38-mm diameter sphere. The comparison is made with the resonant frequencies in the high- $\omega_c \tau$ limit (Table I). Since the detector was not an infinite solenoid (see Appendix C), an octupole contribution to the signal was present which may distort the observed resonances. The particular method of locating the resonant frequency is also important. In light of these comments, we regard the agreement as excellent. Although signal amplitude data are not given by Rose, his comments "strong" and "weak" on the relative amplitudes is in agreement with our classification "fundamental" and "satellite."

In Fig. 12 we show some preliminary data on a spherical sample of potassium metal at 4.2 K in a field of 2500 G. The sample's resistivity ratio is about 3000 and its diameter is 3.8 mm. The solid and dashed curves are the results of a theoretical calculation of the induced magnetic dipole moment. The circles and triangles are data

TABLE I. Resonant frequencies. $V_r/W = 4\pi\omega_r\sigma a^2/c^2\omega_c\tau$.

Resonance	Transverse V_r/W	Longitudinal V_r/W
(1, 0)	4.9020 ± 0.0002	...
(1, 1)	10.58 ± 0.01	21.781 ± 0.005
(1, 2)	16.45 ± 0.01	33.29 ± 0.02
(1, 3)	22.42 ± 0.02	45.05 ± 0.03
(2, 0)	30.35 ± 0.02	...
(2, 1)	47.02 ± 0.02	...
(2, 2)	64.10 ± 0.02	62.21 ± 0.01
(2, 3)	...	84.24 ± 0.04
(3, 0)	75.21 ± 0.01	...
(3, 1)	102.4 ± 0.3	...
(4, 0)	139.75 ± 0.01	...

TABLE II. Dipole-moment numerical convergence.

Resonance	W	N = 11		N = 13		N = 15	
		V_r/W	Peak	V_r/W	Peak	V_r/W	Peak
Transverse geometry							
(1, 2)	40	16.5395	0.3242	16.5460	0.3242	16.5417	0.3241
	100	16.4665	0.5640	16.4668	0.5622	16.4661	0.5586
(2, 0)	40	30.4046	2.1784	30.4035	2.1875	30.4027	2.1843
	100	30.3473	4.9743	30.3585	5.2112	30.3540	5.2106
Longitudinal geometry							
(1, 1)	40	21.8362	0.4849	21.8362	0.4849	21.8296	0.4849
	100	21.7906	1.1589	21.7870	1.1597	21.7907	1.1590
(1, 3)	40	45.5504	0.1090	45.3267	0.1035	45.3297	0.1031
	100	45.4140	0.2110	45.1126	0.1912	45.0767	0.1884

points. The ordinate was scaled so that the peak of the first resonance matched the data in millivolts. The abscissa scale and the choice of $\omega_c \tau$ were adjusted so that the resonant frequency and width of the first peak matched the experimental data. Thus, we have forced the large peak in $\text{Im}M_x$ to agree with experiment. The detailed agreement with theory is impressive: The long tail on the first resonance, the location and size of the second resonance, and the diffuse character of the third resonance are all accurately predicted. The corresponding structure in $\text{Re}M_x$, for which no adjustments have been made, is predicted almost precisely.

The small deviations of the data from the theory may be due to the octupole field. The detector was a pair of coils placed on either side of the sample, with their axes along \hat{y} . The octupole contribution to the signal does not cancel for this detector. At this low field, calculation shows that the octupole field is small, but nevertheless of the order of the deviations seen in Fig. 12. It should be pointed

out that the value of σ inferred from the fitting procedure used here is somewhat smaller than the value σ_0 as measured from the ratio of the in-phase to the out-of-phase signals in zero dc field. This is due to magnetoresistance. We will defer a discussion of our current and continuing measurements on the magnetoresistance of potassium metal to a later paper.

VII. CONCLUDING REMARKS

Our purpose in treating this problem in such great detail has been to allow a direct unambiguous quantitative analysis of helicon experiments, which are necessarily performed on finite geometry samples. The reason such experiments are interesting is that they can give a precision contactless measurement of the magnetic field dependence of the resistivity and the Hall coefficient for the alkali metals. The observed high-field nonsaturating magnetoresistance of potassium remains a fundamental problem of metal physics.¹⁵

There are a number of extensions of our calcu-

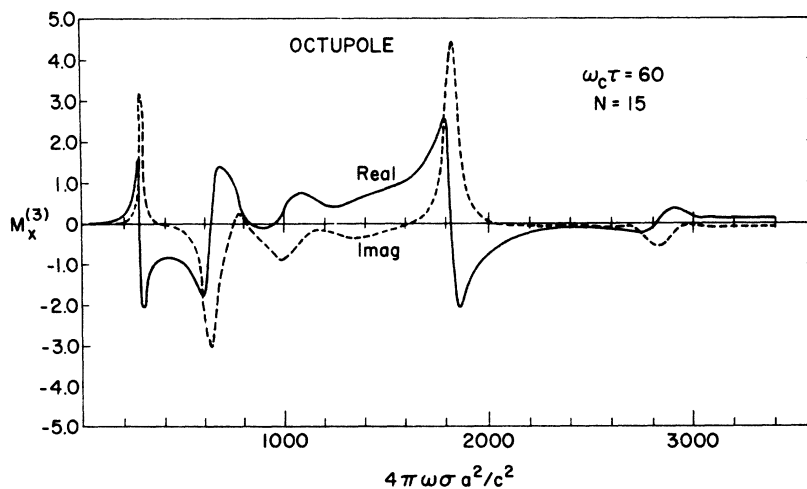


FIG. 9. x component of the induced octupole moment as a function of $V = 4\pi\omega\sigma a^2/c^2$ for $\omega_c\tau = 60$ for the transverse geometry. The ordinate is $M_x^{(3)}$ in units of $\frac{1}{4}B_1 a^5$ as given by Eq. (82).

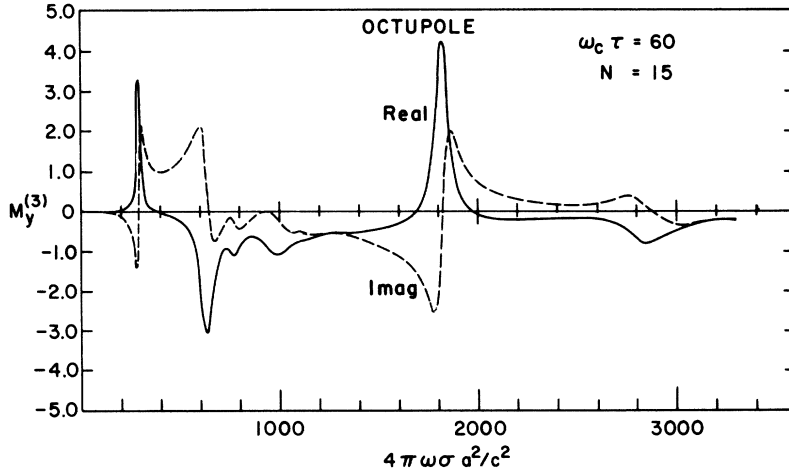


FIG. 10. y component of the induced octupole moment in units of $\frac{1}{4}B_1 a^5$, for $\omega_c\tau=60$ for the transverse geometry as a function of $V=4\pi\omega\sigma a^2/c^2$.

lations which we have not pursued and which would be of interest. One expects there exist simple analytical expressions for the resonance structure at high magnetic fields, e. g., the linear growth of the peak heights and Q 's of the resonances. The answer to this and similar questions might be found by studying the free helicon oscillations of the sphere, which are related to the zeros of the denominator determinant in Eq. (52). It would also be interesting to explore other techniques of solution of Eq. (48) as we suggested in Sec. III D.

We would like to point out three related problems of interest. It would clearly be important if one could extend the calculations to include an anisotropic conductivity of the sample. Nonlocal effects, which we have neglected, would be important if the electron mean free path were comparable to the radius of the sphere. Finally, we have neglected quantum effects, i. e., the deHaas-van Alphen and Shubnikov-deHaas effects.

ACKNOWLEDGMENTS

We wish to thank A. W. Overhauser and T. K.

Hunt for their stimulating interest and for their careful reading of the manuscript. One of us (S. A. W.) would also like to acknowledge a very useful discussion with A. Gold on his and S. Feser's work on this problem.

APPENDIX A: SPHERICAL BESSEL FUNCTIONS

The spherical Bessel functions¹⁶ are solutions of the differential equation:

$$\frac{d^2u}{d\rho^2} + \frac{2}{\rho} \frac{du}{d\rho} + \left(1 - \frac{l(l+1)}{\rho^2}\right)u = 0, \quad (\text{A1})$$

where l is a non-negative integer. The solutions regular at $\rho=0$ are given by the Rodrigues formula

$$j_l(\rho) = \rho^l \left(-\frac{1}{\rho} \frac{d}{d\rho}\right)^l \frac{\sin\rho}{\rho}. \quad (\text{A2})$$

Their relation to the ordinary Bessel functions of half-odd integer order is

$$j_l(\rho) = (\pi/2\rho)^{1/2} J_{l+1/2}(\rho). \quad (\text{A3})$$

Their behavior for small ρ may be inferred from the formula

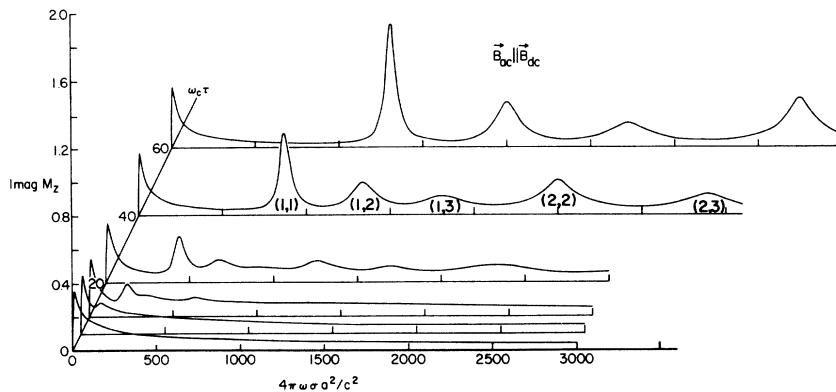


FIG. 11. Development of the helicon resonant structure with increasing $\omega_c\tau$ for the longitudinal geometry. $\text{Im}M_z$ is in units of $\frac{1}{2}B_1 a^3$. The resonance indexing scheme is given by Eq. (80). Compare the amplitudes of the resonances here with those in Fig. 6 and 7, noting the difference in scale between these figures.

TABLE III. Comparison of theoretical resonant frequencies with the experiments of Rose (Ref. 14) on Na spheres at 4.2 K in a field of 50 kG. The numbers given are normalized to the first (1, 0) resonance.

Resonance	Sphere diam = 9.63 mm	Sphere diam = 6.38 mm	Comment	Theory
(1, 0)	1.000	1.000	strong	1.000
(1, 1)	2.27	2.2	weak	2.158
(1, 2)	3.35	3.4	weak	3.356
(1, 3)		4.574
(2, 0)	6.41	6.3	strong	6.191
(2, 1)	10.1	9.7	weak	9.592
(2, 2)		13.08
(3, 0)	15.9	16.	strong	15.34
(3, 1)	22.0	22.	weak	20.89
(4, 0)	29.5	...	strong	28.51

$$j_l(\rho) = \left(\frac{1}{2}\rho\right)^l \frac{\Gamma(\frac{3}{2})}{\Gamma(l+\frac{3}{2})} {}_0F_1\left(l+\frac{3}{2}; -\frac{1}{4}\rho^2\right). \quad (\text{A4})$$

For large ρ their behavior may be inferred from the formula

$$j_l(\rho) = \rho^{-1} [P_l(\rho) \sin(\rho - \frac{1}{2}l\pi) + Q_l(\rho) \cos(\rho - \frac{1}{2}l\pi)], \quad (\text{A5})$$

where

$$P_l(\rho) = \sum_{k=0}^{[l/2]} (-)^k \frac{(l+2k)!}{(2k)!(l-2k)!} (2\rho)^{-2k}, \quad (\text{A6})$$

$$Q_l(\rho) = \sum_{k=0}^{[(l-1)/2]} (-)^k \frac{(l+2k+1)!}{(2k+1)!(l-2k-1)!} (2\rho)^{-2k-1}.$$

The spherical Bessel functions satisfy the recursion relations

$$j_{l+1}(\rho) + j_{l-1}(\rho) = [(2l+1)/\rho] j_l(\rho), \quad (\text{A7})$$

$$j_{l-1}(\rho) = \rho^{-l-1} \frac{d}{d\rho} \rho^{l+1} j_l(\rho). \quad (\text{A8})$$

$$j_{l+1}(\rho) = -\rho^l \frac{d}{d\rho} \rho^{-l} j_l(\rho). \quad (\text{A9})$$

For further details see the references.

APPENDIX B: VECTOR SPHERICAL HARMONICS

The vector spherical harmonics¹⁷ are constructed from the complex basis vectors

$$\hat{e}_1 = -2^{-1/2}(\hat{x} + i\hat{y}), \quad \hat{e}_0 = \hat{z}, \quad \hat{e}_{-1} = 2^{-1/2}(\hat{x} - i\hat{y}), \quad (\text{B1})$$

and the usual (scalar) spherical harmonics:

$$Y_l^m(\theta, \varphi) = (-1)^m \left(\frac{2l+1}{4\pi} \frac{(l-m)!}{(l+m)!} \right)^{1/2} P_l^m(\cos\theta) e^{im\varphi}, \quad (\text{B2})$$

in which P_l^m is the associated Legendre polynomial defined by the Rodrigues formula

$$P_l^m(x) = \frac{(1-x^2)^{m/2}}{2^l l!} \frac{d^{l+m}}{dx^{l+m}} (x^2-1)^l. \quad (\text{B3})$$

The vector spherical harmonics are defined by

$$\begin{aligned} \vec{Y}_{l+1,l}^m = & \left(\frac{(l+m)(l+m+1)}{2(l+1)(2l+1)} \right)^{1/2} Y_l^{m-1} \hat{e}_1 \\ & + \left(\frac{(l-m+1)(l+m+1)}{(l+1)(2l+1)} \right)^{1/2} Y_l^m \hat{e}_0 \\ & + \left(\frac{(l-m)(l-m+1)}{2(l+1)(2l+1)} \right)^{1/2} Y_l^{m+1} \hat{e}_{-1}, \quad (\text{B4}) \end{aligned}$$

$$\begin{aligned} \vec{Y}_{l,l}^m = & - \left(\frac{(l+m)(l-m+1)}{2l(l+1)} \right)^{1/2} Y_l^{m-1} \hat{e}_1 + \frac{m}{[l(l+1)]^{1/2}} Y_l^m \hat{e}_0 \\ & + \left(\frac{(l-m)(l+m+1)}{2l(l+1)} \right)^{1/2} Y_l^{m+1} \hat{e}_{-1}, \quad (\text{B5}) \end{aligned}$$

$$\begin{aligned} \vec{Y}_{l-1,l}^m = & \left(\frac{(l-m)(l-m+1)}{2l(2l+1)} \right)^{1/2} Y_l^{m-1} \hat{e}_1 \\ & - \left(\frac{(l-m)(l+m)}{l(2l+1)} \right)^{1/2} Y_l^m \hat{e}_0 \\ & + \left(\frac{(l+m)(l+m+1)}{2l(2l+1)} \right)^{1/2} Y_l^{m+1} \hat{e}_{-1}. \quad (\text{B6}) \end{aligned}$$

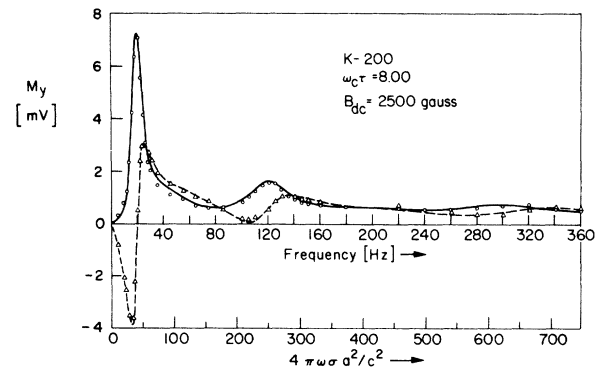


FIG. 12. Comparison of the results of an experiment on a small sphere ($a \approx 1.9$ mm) of potassium metal at 4.2 K with theory. The experiment was done in the so-called "crossed-coil" configuration in which the dc field is along \hat{z} , the applied ac field along \hat{x} , and the y component of \vec{M} is measured. The dashed line is the imaginary part and the solid line is the real part of M_y .

Equivalent definitions are

$$r^l \bar{Y}_{l+1,l}^m = \frac{1}{[(l+1)(2l+3)]^{1/2}} \bar{\nabla} r^{l+1} Y_{l+1}^m(\theta, \varphi), \quad (B7)$$

$$r^l \bar{Y}_{l,l}^m = -i \frac{1}{[l(l+1)]^{1/2}} \bar{\nabla} \times \bar{\nabla} r^l Y_l^m(\theta, \varphi), \quad (B8)$$

$$r^{-l-1} \bar{Y}_{l-1,l}^m = \frac{1}{[l(2l-l)]^{1/2}} \bar{\nabla} r^{-l} Y_{l-1}^m(\theta, \varphi). \quad (B9)$$

The orthogonality relation for the vector spherical harmonics is

$$\int_0^{2\pi} d\varphi \int_0^\pi d\theta \sin\theta \bar{Y}_{L',l'}^{M',*} \cdot \bar{Y}_{L,l}^M = \delta_{L'L} \delta_{l'l} \delta_{m'm}. \quad (B10)$$

They have the following simple vector analytical properties:

$$\text{div}R(r) \bar{Y}_{l,l+1}^m = -\left(\frac{l+1}{2l+1}\right)^{1/2} r^{-l-2} \frac{d}{dr} r^{l+2} R(r) Y_l^m(\theta, \varphi),$$

$$\text{div}R(r) \bar{Y}_{l,l}^m = 0, \quad (B11)$$

$$\text{div}R(r) \bar{Y}_{l,l-1}^m = \left(\frac{l}{2l+1}\right)^{1/2} r^{-l-1} \frac{d}{dr} r^{-l+1} R(r) Y_l^m(\theta, \varphi),$$

and

$$\begin{aligned} \text{curl}R(r) \bar{Y}_{l,l+1}^m &= i \left(\frac{l}{2l+1}\right)^{1/2} r^{-l-2} \frac{d}{dr} r^{l+2} R(r) \bar{Y}_{l,l}^m, \\ \text{curl}R(r) \bar{Y}_{l,l}^m &= i \left(\frac{l}{2l+1}\right)^{1/2} r^l \frac{d}{dr} r^{-l} R(r) \bar{Y}_{l,l+1}^m \\ &\quad + i \left(\frac{l+1}{2l+1}\right)^{1/2} r^{-l-1} \frac{d}{dr} r^{l+1} R(r) \bar{Y}_{l,l-1}^m, \\ \text{curl}R(r) \bar{Y}_{l,l-1}^m &= i \left(\frac{l+1}{2l+1}\right)^{1/2} r^{l-1} \frac{d}{dr} r^{-l+1} R(r) \bar{Y}_{l,l}^m. \end{aligned} \quad (B12)$$

Also useful is the formula

$$\begin{aligned} \bar{\nabla} R(r) Y_l^m(\theta, \varphi) &= -\left(\frac{l+1}{2l+1}\right)^{1/2} r^l \frac{d}{dr} r^{-l} R(r) \bar{Y}_{l,l+1}^m \\ &\quad + \left(\frac{l}{2l+1}\right)^{1/2} r^{-l-1} \frac{d}{dr} r^{l+1} R(r) \bar{Y}_{l,l-1}^m. \end{aligned} \quad (B13)$$

With the aid of the simple result

$$\hat{z} \times \hat{e}_m = -im \hat{e}_m, \quad (B14)$$

we can show from (B4)–(B6) that

$$\begin{aligned} i \hat{z} \times \bar{Y}_{l+1,l}^m &= \frac{m}{l+1} \bar{Y}_{l+1,l}^m - \left(\frac{l(l-m+1)(l+m+1)}{(l+1)^2(2l+1)}\right)^{1/2} \bar{Y}_{l,l}^m, \\ i \hat{z} \times \bar{Y}_{l,l}^m &= -\left(\frac{l(l-m+1)(l+m+1)}{(l+1)^2(2l+1)}\right)^{1/2} \bar{Y}_{l+1,l}^m \\ &\quad + \frac{m}{l(l+1)} \bar{Y}_{l,l}^m \\ &\quad - \left(\frac{(l+1)(l-m)(l+m)}{l^2(2l+1)}\right)^{1/2} \bar{Y}_{l-1,l}^m \end{aligned}$$

$$i \hat{z} \times \bar{Y}_{l-1,l}^m = -\left(\frac{(l+1)(l-m)(l+m)}{l^2(2l+1)}\right)^{1/2} \bar{Y}_{l,l}^m - \frac{m}{l} \bar{Y}_{l-1,l}^m.$$

APPENDIX C: DETECTOR COUPLING COEFFICIENTS

Consider first the coupling of the dipole and octupole fields to a single-loop coil of radius R placed a distance h from the center of the sphere. We take the coil to be oriented so that the plane containing the loop is perpendicular to the line joining the center of the sphere and the center of the coil.

According to Eq. (42) the dipole ($l=1$), octupole ($l=3$), and higher-moment magnetic fields outside the sphere are

$$\bar{\mathbf{B}}^{(l)} = (a/r)^{l+2} \sum_{m=-l}^l F_l^m \bar{Y}_{l,l+1}^m. \quad (C1)$$

The flux threading the coil due to the 2^l -pole moment is

$$\Phi^{(l)} = \int d\bar{\mathbf{A}} \cdot \bar{\mathbf{B}}^{(l)}. \quad (C2)$$

Using Eq. (C1), the definition (62) of the multipole moment vector, and the formulas in Appendix B, we find for the dipole flux

$$\Phi^{(1)} = 2\pi \hat{h} \cdot \bar{\mathbf{M}}^{(1)} \frac{R^2}{(R^2 + h^2)^{3/2}}, \quad (C3)$$

and for the octupole flux

$$\begin{aligned} \Phi^{(3)} &= -\frac{\pi R^2 (R^2 - 4h^2)}{8^{1/2} (R^2 + h^2)^{7/2}} \{ [5(\hat{z} \cdot \hat{h})^2 - 3] \hat{z} \cdot \hat{h} \hat{z} \cdot \bar{\mathbf{M}}^{(3)} \\ &\quad + (\frac{3}{2})^{1/2} [5(\hat{z} \cdot \hat{h})^2 - 1] \hat{h} \cdot (\bar{\mathbf{M}}^{(3)} - \hat{z} \cdot \bar{\mathbf{M}}^{(3)} \hat{z}) \}, \end{aligned} \quad (C4)$$

where \hat{h} is a unit vector normal to the plane of the coil. The dipole moment $\bar{\mathbf{M}} \equiv \bar{\mathbf{M}}^{(1)}$.

Consider now a solenoid of radius R , length $2H$, n turns per unit length, with its axis along \hat{h} , and the sphere placed at its center. The signal due to the 2^l -pole moment is

$$V^{(l)} = i\omega n \int_{-H}^H dh \Phi^{(l)}. \quad (C5)$$

We find for the dipole field

$$V^{(1)} = i4\pi\omega n \hat{h} \cdot \bar{\mathbf{M}}^{(1)} [H/(R^2 + H^2)^{1/2}], \quad (C6)$$

and for the octupole field

$$\begin{aligned} V^{(3)} &= -\frac{i\pi\omega n}{2^{1/2}} \frac{HR^2}{(R^2 + H^2)^{5/2}} \{ [5(\hat{z} \cdot \hat{h})^2 - 3] \hat{z} \cdot \hat{h} z \cdot \bar{\mathbf{M}}^{(3)} \\ &\quad + (\frac{3}{2})^{1/2} [5(\hat{z} \cdot \hat{h})^2 - 1] \hat{h} \cdot (\bar{\mathbf{M}}^{(3)} - \hat{z} \cdot \bar{\mathbf{M}}^{(3)} \hat{z}) \}. \end{aligned} \quad (C7)$$

$V^{(l)}$ will be in volts if B_1 is in Wb/m^2 and all lengths are in meters. Note that the signal due to the octupole moment is zero for an infinite solenoid. This is, of course, also true for the higher moments.

- ¹Electromagnetic waves in the ionosphere of the helicon type which are now called whistlers were identified long ago by Barkhausen [Phys. Z. **20**, 401 (1919)]. The name "helicon" was given to these oscillations by P. Aigrain [in *Proceedings of the International Conference on Semiconductor Physics*, Prague, 1960 (Academic, New York, 1961), p. 244] when he predicted they should occur in semiconductors. They were first observed in metals (Na) by R. Bowers, C. Legendy, and F. Rose [Phys. Rev. Lett. **7**, 339 (1961)].
- ²B. W. Maxfield, Am. J. Phys. **37**, 241 (1969).
- ³W. R. Smythe, *Static and Dynamic Electricity* (McGraw-Hill, New York, 1950), p. 397.
- ⁴J. E. Zimmerman, Rev. Sci. Instrum. **32**, 402 (1960).
- ⁵Essentially these same functions are frequently used in solving the vector wave equation in spherical coordinates. See, e.g., P. M. Morse and H. Feshbach, *Methods of Theoretical Physics* (McGraw-Hill, New York, 1953), p. 1864.
- ⁶See, for example, F. B. Hildebrand, *Methods of Applied Mathematics*, 2nd. ed. (Prentice-Hall, Englewood Cliffs, N. J., 1962), p. 10.
- ⁷Bateman Manuscript Project, *Higher Transcendental Functions*, edited by A. Erdelyi (McGraw-Hill, New York, 1953), Vol. 2.
- ⁸A. R. Edmonds, *Angular Momentum in Quantum Mechanics* (Princeton U. P., Princeton, N. J., 1951).
- ⁹See, for example, R. Courant and D. Hilbert, *Methods of Mathematical Physics*, 1st English ed. (Interscience, New York, 1953), Vol. I, Chap. III.
- ¹⁰The low-frequency results obtained here have also been obtained directly from the basic equations (1), (2), and (3) using a perturbation expansion in the parameter V .
- ¹¹See, for example, J. Moss and W. R. Datars, Phys. Lett. A **24**, 630 (1967); and J. S. Lass, and A. B. Pippard, J. Phys. E **3**, 139 (1970).
- ¹²This indexing scheme was proposed by A. Gold and S. Feser (private communication).
- ¹³This geometry has been considered by J. L. A. Francey and D. J. Gates [J. Phys. A **1**, 710 (1968)] for the special case of zero resistivity. Their procedure is to expand the magnetic field inside the sphere in cylindrical waves. The approximate values for the resonant frequencies which they give are considerably different from the exact results (Table I).
- ¹⁴F. Rose, Ph.D. thesis (Cornell University, 1965) (unpublished).
- ¹⁵See, for example, E. Justi, Ann. Phys. (Leipz.) **3**, 183 (1948); D. K. C. Mac Donald, *Handbuch der Physik* (Springer-Verlag, Berlin, 1956), Vol. 14, p. 137; P. A. Penz and R. Bowers, Solid State Commun. **5**, 341 (1967); J. Babiskin and P. G. Siebermann, Phys. Rev. Lett. **27**, 1361 (1971); H. Taub, R. L. Schmidt, B. W. Maxfield, and R. Bowers, Phys. Rev. B **4**, 1471 (1971).
- ¹⁶See, for example, M. Abramowitz and I. A. Stegun, *Handbook of Mathematical Functions*, NBS Applied Mathematics Series No. 55 (U. S. GPO, Washington, 1964); or L. I. Schiff, *Quantum Mechanics* (McGraw-Hill, New York, 1955), p. 77.
- ¹⁷See Ref. 8, pp. 81-85; J. M. Blatt and V. F. Weiskopf, *Theoretical Nuclear Physics* (Wiley, New York, 1952), Appendix B.